RSC Chemical Biology

Check for updates

A silicon-rhodamine chemical-genetic hybrid for far red voltage imaging from defined neurons in brain slice†

Gloria Ortiz,[a] Pei Liu,[a] Parker E. Deal, [ID][a] Ashley K. Nensel,[a] Kayli N. Martinez,[a] Kiarash Shamardani, [ID][b] Hillel Adesnik[bc] and Evan W. Miller [ID] ⋆[abc]

We describe the design, synthesis, and application of voltage-sensitive silicon rhodamines. Based on the Berkeley Red Sensor of Transmembrane potential, or BeRST, scaffold, the new dyes possess an isomeric molecular wire for improved alignment in the plasma membrane and 2′ carboxylic acids for ready functionalization. The new isoBeRST dyes have a voltage sensitivity of 24% $\Delta F/F$ per 100 mV. Combined with a flexible polyethyleneglycol (PEG) linker and a chloroalkane HaloTag ligand, isoBeRST dyes enable voltage imaging from genetically defined cells and neurons and provide improved labeling over previous, rhodamine-based hybrid strategies. isoBeRST-Halo hybrid indicators achieve single-trial voltage imaging of membrane potential dynamics from cultured hippocampal neurons or cortical neurons in brain slices. With far-red/near infrared excitation and emission, turn-on response to action potentials, and effective cell labeling in thick tissue, the new isoBeRST-Halo derivatives provide an important complement to voltage imaging in neurobiology.

voltage-sensitive fluorophore, Berkeley Red Sensor of Transmembrane potential 1, or BeRST 1, a silicon-rhodamine-based indicator that operates *via* voltage-sensitive photoinduced electron transfer (PeT)[25] and provides a faithful readout of fast voltage changes, outperforming completely genetically encoded voltage indicators.[26] The high sensitivity (24% $\Delta F/F$ per 100 mV), fast response kinetics, photostability, and far red/near infra-red excitation and emission profile enable the use of BeRST 1 in a number of voltage imaging applications.[27–29]
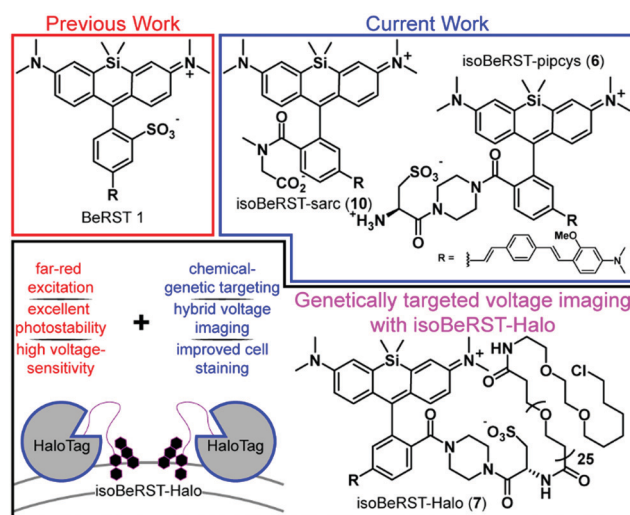
However, the use of BeRST 1 has been largely restricted to *in vitro* systems of homogeneous cell types because, unlike genetically encoded indicators, BeRST cannot be targeted to specific cells. Usage in more complex settings, like thick brain tissue, remains a challenge because of a lack of methods to genetically target BeRST 1 to defined cells (Scheme 1). Here we report two new synthetic BeRST dyes and show that this new class of indicator can be combined with a genetically-encoded

Introduction

Voltage imaging in the central nervous system promises to transform the ways in which we observe brain systems.[1,2] Recently, a number of approaches to voltage imaging have emerged, including methods that rely solely on synthetic dyes[3–9] or genetically encoded proteins.[10–17] Alternatively, hybrid methodologies can combine the unique properties of synthetic dyes—high molecular brightness, wide availability of colors, or fast response kinetics—with the cellular specificity of genetically encoded methods.[18–24] Our group recently reported the development of a completely synthetic

[a] *Department of Chemistry, University of California, Berkeley, California, 94720-1460, USA. E-mail: evanwmiller@berkeley.edu*

[b] *Department of Molecular & Cell Biology, University of California, Berkeley, California, 94720-1460, USA*

[c] *Helen Wills Neuroscience Institute, University of California, Berkeley, California, 94720-1460, USA*

† Electronic supplementary information (ESI) available: Spectra, supporting figures, experimental details. See DOI: 10.1039/d1cb00156f

Scheme 1 Overview of isoBeRST-Halo.

protein tether to enable voltage imaging from defined cells in mouse brain slice.

Results

To enable genetic targeting of BeRST-style dyes, we redesigned the synthesis of BeRST. We replaced the 2′-sulfonate of BeRST with a carboxylate: this allows for addition of covalent tethers and mimics our previous design success with Rhodamine-based Voltage Reporters (RhoVRs).[30,31] We also used the 5′ version of molecular wire, since the 5′, or isomeric, version showed improved voltage sensitivity compared to the 4′ RhoVR.[30] Additionally, the commercial availability of the precursors to the aldehyde starting material substantially simplified the synthetic route (Scheme S1, ESI†). The optimized synthesis of isoBeRST-sarc 10 begins with a Heck reaction between fluorophore 1[34,35] and (E)-3-methoxy-N,N-dimethyl-4-(4-vinylstyryl)aniline[36] to obtain carboxy silicon rhodamine 8 (Scheme S1, ESI†). Dye 8 is coupled to sarcosine tert-butyl ester using oxalyl chloride, followed by a TFA-catalyzed deprotection of the tert-butyl ester to give the voltage-sensitive fluorophore isoBeRST-sarc 10, which is the Si-rhodamine analog of RhoVR 1.[30]
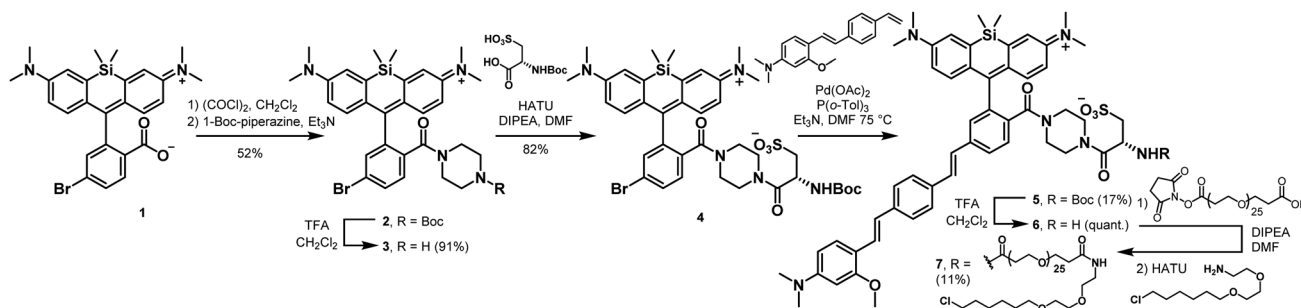
We also synthesized the piperazine-cysteic acid conjugate of isoBeRST, or isoBeRST-pipcys 6, since this configuration allowed us to target RhoVR dyes to specific cells using HaloTag (Scheme 2).[31] The synthesis of isoBeRST-pipcys 6 and isoBeRST-Halo 7 follows a sequential amide-coupling/Heck coupling sequence. This provided higher overall yields than amide coupling with the assembled molecular wire/fluorophore 8. The cyclic, piperazine-derived tertiary amide of 3 appears more stable than the amide formed from sarcosine, based on its ability to undergo successful Pd-catalyzed synthesis of isoBeRST-pipcys 6. The route begins with oxalyl chloride mediated coupling of reported silicon rhodamine 1 with 1-Boc-piperazine, followed by TFA deprotection to yield silicon rhodamine 2 (Scheme 2). A second coupling mediated by HATU installed Boc-L-cysteic acid, affording 3. Compound 3 was then submitted to a Heck reaction with (E)-3-methoxy-N,N-dimethyl-4-(4-vinylstyryl)aniline to provide 5. Subsequent TFA deprotection gives voltage-sensitive fluorophore isoBeRST-pipcys 6 in 17% yield. In a one-pot sequence, isoBeRST-pipcys 6 is reacted with acid-dPEG25-NHS ester, followed by addition of HaloTag amine[37] (Scheme 2) and HATU. The complete reaction was purified via preparative-scale HPLC to yield the genetically-targetable isoBeRST-Halo 7 in

11% yield. We selected a PEG25 linker because, for RhoVR-Halo, a PEG$_n$ linker with $n = 25$ monomer units almost completely recovered the full voltage sensitivity of the untethered, parent indicator (34% $\Delta F/F$ vs. 38% $\Delta F/F$).[31] Shorter PEG linkers ($n = 13$, 9, or 5) had lower voltage sensitivity, and PEG$_0$ had no voltage sensitivity.

Spectroscopic characterization of isoBeRST-sarc 10, isoBeRST-pipcys 6, and isoBeRST-Halo 7 reveals that all three voltage indicators possess similar photophysical properties (Table 1, Fig. 1, Fig. S1 and S2, ESI†). IsoBeRST-sarc 10 displays a λ_{max} at 661 nm, similar to BeRST 1 (λ_{max} = 658 nm) and identical to isoBeRST-pipcys 6 and isoBeRST-Halo 7. IsoBeRST-sarc 10 possesses an emission maximum of 681 nm and a quantum yield (Φ) of 8.0%, while isoBeRST-pipcys 6 has an emission maximum of 681 nm and Φ of 5.0%. IsoBeRST-Halo 7 has an emission maximum of 677 nm and Φ of 3.4%.

All of the new Si-rhodamine indicators are voltage-sensitive. In human embryonic kidney (HEK) cells untargeted dyes isoBeRST-sarc 10 (Fig. S1, ESI†) and isoBeRST-pipcys 6 (Fig. S2, ESI†) localize to the plasma membrane and are voltage sensitive. IsoBeRST-pipcys 6 has a voltage sensitivity of 24% ± 2% $\Delta F/F$ per 100 mV (SNR = 110 ± 15), identical to BeRST 1 (24% ± 5% $\Delta F/F$ per 100 mV)[25] and to isoBeRST-sarc 10 (Table 1). We selected isoBeRST-pipcys 6 to evaluate in neurons because of the higher yielding synthesis and stability compared to isoBeRST-sarc 10. In cultured rat hippocampal neurons, isoBeRST-pipcys 6 (500 nM) provided clear resolution of action potentials (Fig. S3, ESI†).

The genetically-targetable isoBeRST-Halo 7 selectively labels HEK cells expressing cell-surface HaloTag (Fig. 1 and Fig. S4, ESI†). We expressed HaloTag on the surface of mammalian cells using a fusion with a single-pass transmembrane domain.[31] At 500 nM isoBeRST-Halo 7, cells expressing cell-surface HaloTag are approximately 14 fold brighter than un-transfected control cells (Fig. S4f, ESI†). At lower concentrations (50 nM), fluorescence intensity in HaloTag-expressing cells increases to approximately 30 fold over non-HaloTag expressing cells (Fig. S4f, ESI†). This is three times better contrast than RhoVR-Halo labeling (10–15 fold).[31] Although expression levels of HaloTag vary with transient transfection, a screen of isoBeRST-Halo 7 concentrations reveals that HaloTag binding sites saturate at around 50 to 100 nM (Fig. S4f, ESI†). The drop in contrast ratio, from ~30 fold at 50 nM to 14 fold at 500 nM

Scheme 2 Synthesis of isoBeRST–pipcys (6) and isoBeRST–Halo (7).

© 2021 The Author(s). Published by the Royal Society of Chemistry

RSC Chem. Biol., 2021, 2, 1594–1599 | 1595

Table 1 Properties of isoBeRST indicators

Compound	$\lambda_{max}{}^a$ nm^{-1}	$\lambda_{em}{}^a$ nm^{-1}	ε^a	Φ^{ab}	% $\Delta F/F$/100 mV^c	Relative brightness^d (%)
isoBeRST-pipcys **6**	662	681	172 000	0.050	24 ± 1.9	100
isoBeRST-Halo **7**	662	677	—	0.034	21 ± 1.2	30
isoBeRST-sarc **10**	661	681	107 700	0.080	24 ± 2.6	—

^{a} In PBS, pH 7.4, 0.1% SDS. ^{b} Referenced to Cy5.5-carboxylic acid in PBS, (Φ = 0.23).[32,33] ^{c} Voltage-clamped HEK cells. Error is ± S.D. for n = 5–6 cells. ^{d} In HEK cells. Error is ± S.E.M for n = 4 coverslips (>100 cells per coverslip for relative brightness).

comes from a small increase in background staining in control cells (an increase of about 4 percentage points, from 5% to 9%). Importantly, isoBeRST-Halo **7** (50 nM) is voltage-sensitive, with a voltage sensitivity of 21% ± 1% $\Delta F/F$ per 100 mV and an SNR of 42 ± 7 (Fig. 1 and Table 1). IsoBeRST-Halo **7** maintains about the same voltage sensitivity as isoBeRST-pipcys **6** (500 nM), indicating that the covalently tethered dye remains properly oriented in the plasma membrane (Table 1 and Fig. 1).

Covalently-tethered isoBeRST-Halo **7** visualizes voltage changes in genetically-defined neurons. Dissociated, cultured rat hippocampal neurons transfected with HaloTag under control of the synapsin promoter were labeled with 50 nM isoBeRST-Halo. Neurons expressing HaloTag show excellent selectivity, revealing good localization of the dye to the outer membrane (Fig. 2 and Fig. S5, ESI†). The best contrast between
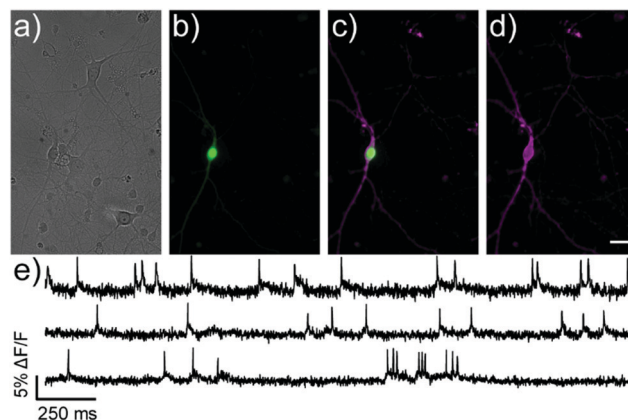

Fig. 2 Monitoring spontaneous activity in neurons with isoBeRST-Halo **7**. (a–d) Wide-field microscopy images of isoBeRST-Halo in a HaloTag-expressing neuron. (a) DIC image of neurons. (b) Nuclear EGFP fluorescence indicates HaloTag expression. (c) Merge of EGFP (green) and isoBeRST-Halo (magenta) fluorescence. (d) isoBeRST-Halo fluorescence is restricted to the membrane. Scale bar is 20 μm. (e) Optical recordings at 500 Hz (1.94 W cm^{-2}) of spontaneous activity shown as $\Delta F/F$ vs. time for HaloTag-expressing neurons from different coverslips labeled with **7**.

HaloTag-expressing and control cells is achieved using 50 nM isoBeRST-Halo (50× brighter than untransfected cells). However, similarly high levels of contrast can be achieved, even when using higher isoBeRST-Halo concentrations (18× to 30× brighter when using 100 to 500 nM isoBeRST-Halo). By comparison, RhoVR-Halo,[31] under identical conditions, can only achieve a selectivity ratio of 9.5× (50 nM RhoVR-Halo), which
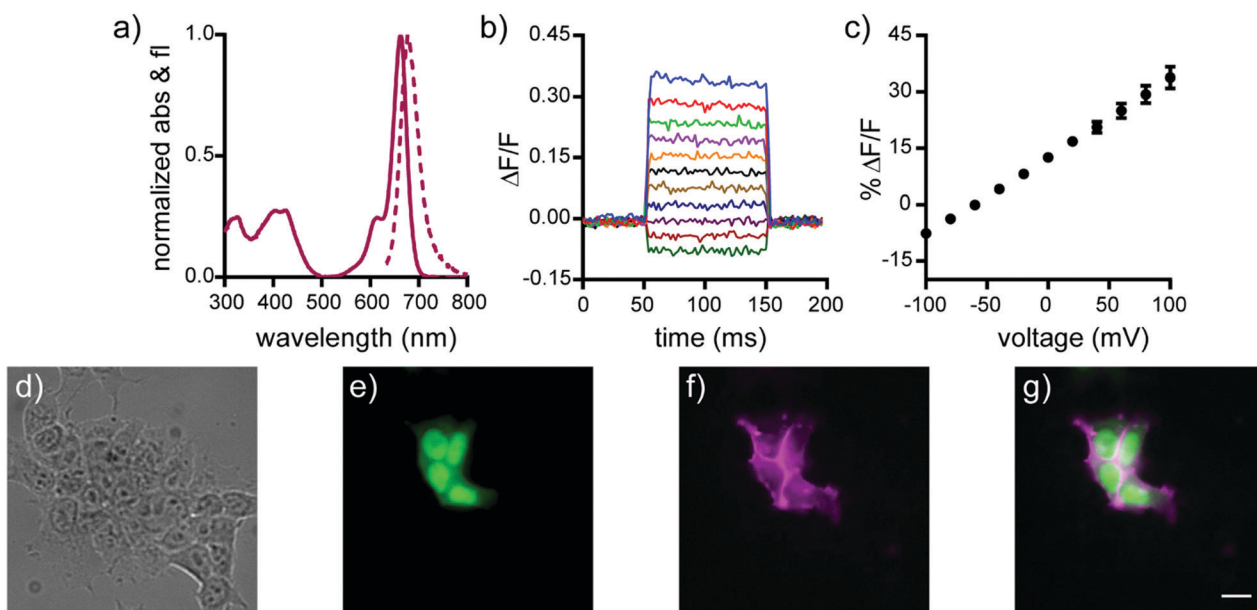

Fig. 1 Cellular and *in vitro* characterization of isoBeRST-Halo **7**. (a) Normalized absorbance (solid line) and emission (dashed line) spectra of isoBeRST-Halo **7** in PBS, pH 7.4. (b) Plot of the fractional change in fluorescence of **7** vs. time for 100 ms hyper- and depolarizing steps (±100 mV in 20 mV increments) from a holding potential of −60 mV for single HEK cells under whole-cell voltage-clamp mode. (c) Plot of % $\Delta F/F$ vs. final membrane potential. Data are mean ±S.D. for n = 6 cells. (d–g) Wide-field microscopy images of HEK cells transfected with CMV-HaloTag-pDisplay and stained with isoBeRST-Halo **7** (50 nM, 30 min). (d) DIC image of HEK cells. (e) Nuclear EGFP fluorescence indicates HaloTag expression. (f) isoBeRST-Halo fluorescence. (g) Merge of fluorescence from EGFP (green) and isoBeRST-Halo (magenta). Scale bar is 10 μm.
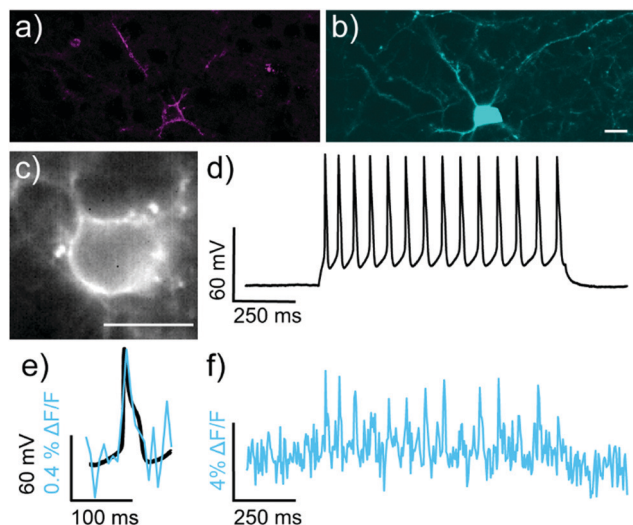
Fig. 3 Characterization of isoBeRST-Halo in mouse brain slice expressing HaloTag-pDisplay and pCAG-BFP. (a and b) Confocal microscopy images of a HaloTag-expressing neuron stained with (a) isoBeRST-Halo (500 nM, 30 min, 23 °C, followed by 2 h in fresh ACSF) and expressing (b) BFP. Scale bar is 20 μm. (c) Wide-field microscopy image of isoBeRST-Halo stained slice acquired during patch-clamp electrophysiology. (d) Plot of voltage vs. time for cell in panel (c). (e) Overlay of membrane potential (black) and isoBeRST-Halo fluorescence (teal). (f) Plot of $\Delta F/F$ fluorescence from isoBeRST-Halo fluorescence for the cell in panel (c). The $\Delta F/F$ trace was acquired at 0.5 kHz and represents single-trial acquisition.

drops to 5× at higher concentrations (200 to 500 nM, Fig. S5f, ESI†). High isoBeRST-Halo fluorescence correlates with high levels of HaloTag/GFP (Fig. S5e–g, ESI†). Using these optimized loading conditions, we demonstrated the ability to record spontaneous and evoked activity in neurons (Fig. 2e and Fig. S6, ESI†). IsoBeRST-Halo responded to field stimulated evoked action potentials with a 10% ± 0.3% $\Delta F/F$ and SNR of 15 ± 1 (19 cells).

We next evaluated the ability of isoBeRST-Halo 7 to monitor voltage dynamics from neurons in brain slice. We introduced genes for HaloTag and a co-expression marker, blue fluorescent protein, or BFP, on separate plasmids via in utero electroporation in mouse embryos.[38] We prepared tissue slices from the brains of these mice and stained the slices with isoBeRST-Halo 7 (250 to 500 nM, 15 min). Confocal fluorescence microscopy reveals localization of isoBeRST-Halo fluorescence in the cell membranes of neurons that express BFP and HaloTag (Fig. 3a and b). Both cell bodies and more distal processes like axonal and dendritic membranes appear fluorescent (Fig. 3a and b and Fig. S7, ESI†), mirroring results in dissociated rat neurons (Fig. 2). Unlabeled cell bodies appear as dark spots, indicating that labeling of neurons requires HaloTag expression (Fig. S7, ESI†). In mouse brain slices, isoBeRST-Halo is voltage-sensitive. Simultaneous patch clamp electrophysiology and fluorescence imaging establishes that isoBeRST-Halo tracks action potentials in a single trial (Fig. 3c–f). The voltage-sensitive fluorescence of isoBeRST-Halo corresponds well with the electrode-based recording of action potentials (Fig. 3e). IsoBeRST-Halo 7 detects action potentials (Fig. 3f) with a SNR of 4.9 ± 1.3 (S.D., n = 10 spikes) and

a $\Delta F/F$ of 3.3% ± 0.6% (S.D., n = 10 spikes). The sensitivity of isoBeRST-Halo 7 in brain slices compares favorably to RhoVR-Halo, which has a higher voltage sensitivity (34%) than isoBeRST-Halo (21%) in HEK cells and has an SNR of 3.3 and a $\Delta F/F$ of 4.3% in brain slice (Table S1, ESI†).[31] IsoBeRST-Halo 7 shows photostability comparable to RhoVR-Halo in brain slice, (Fig. S8 and Table S1, ESI†). This photostability tracks with the photostability measured for the untargeted dyes (isoBeRST-pipcys 6) in HEK 293T cells (Fig. S8, ESI†).

Conclusion

In summary, we describe the design, synthesis, and application of new silicon-rhodamine-based voltage-sensitive fluorophores. The new BeRST derivatives rely on a 2′ carboxylate, rather than sulfonate, and can be combined with secondary amines to generate tertiary amides that function well as voltage indicators in their own right, with $\Delta F/F$ values matching the sulfonate-based BeRST 1.[25] Unlike BeRST 1, however, the new carboxy-containing isoBeRST derivatives reported here can be readily incorporated into a hybrid genetic targeting framework. When combined in this way, isoBeRST-Halo 7 enables selective labeling of cells expressing cell-surface HaloTag, including HEK293T cells, dissociated rat hippocampal neurons, and cortical neurons in mouse brain slices. Labeling with iso-BeRST-Halo provides improved contrast between HaloTag-expressing and non-expressing cells, compared to RhoVR1-Halo (Fig. S5f, ESI†).[31] In all of these contexts, isoBeRST-Halo is voltage-sensitive, with $\Delta F/F$ values comparable to the parent BeRST 1 indicator.

Voltage imaging with isoBeRST-Halo 7 provides an important complement to voltage imaging efforts. It offers a turn-on indicator for action potentials, possesses an excitation spectrum aligned with common excitation sources, operates in the far-red/near infrared some 90 nm red-shifted relative to previous RhoVR1-Halo strategies,[31] and takes advantage of the high photostability of silicon-rhodamines (Table S1, ESI†).[25,39,40] In the future, we will maximize expression of cell-surface HaloTag, since one limitation of the covalent tethering approach is that the stoichiometric labeling limits the number of indicators that can be added to a cell membrane. Finally, we envision that isoBeRST-Halo can pair with optically[31] and enzymatically orthogonal hybrid genetic labeling strategies[41–43] to provide multi-color voltage imaging in complex tissues.

Ethical statement

All animal procedures were approved by the UC Berkeley Animal Care and Use Committees and conformed to the NIH Guide for the Care and Use and Laboratory Animals and the Public Health Policy.

Conflicts of interest

There are no conflicts to declare.

© 2021 The Author(s). Published by the Royal Society of Chemistry

RSC Chem. Biol., 2021, 2, 1594–1599 | 1597

Acknowledgements

Notes and references

1 D. S. Peterka, H. Takahashi and R. Yuste, *Neuron*, 2011, **69**, 9–21.
2 M. Scanziani and M. Häusser, *Nature*, 2009, **461**, 930–939.
3 P. Liu and E. W. Miller, *Acc. Chem. Res.*, 2020, **53**, 11–19.
4 N. A. Sayresmith, A. Saminathan, J. K. Sailer, S. M. Patberg, K. Sandor, Y. Krishnan and M. G. Walter, *J. Am. Chem. Soc.*, 2019, **141**, 18780–18790.
5 J. E. Reeve, A. D. Corbett, I. Boczarow, W. Kaluza, W. Barford, H. Bayley, T. Wilson and H. L. Anderson, *Angew. Chem., Int. Ed.*, 2013, **52**, 9044–9048.
6 C. E. Rowland, K. Susumu, M. H. Stewart, E. Oh, A. J. Mäkinen, T. J. O'Shaughnessy, G. Kushto, M. A. Wolak, J. S. Erickson, A. L. Efros, A. L. Huston and J. B. Delehanty, *Nano Lett.*, 2015, **15**, 6848–6854.
7 P. Yan, C. D. Acker, W. L. Zhou, P. Lee, C. Bollensdorff, A. Negrean, J. Lotti, L. Sacconi, S. D. Antic, P. Kohl, H. D. Mansvelder, F. S. Pavone and L. M. Loew, *Proc. Natl. Acad. Sci. U. S. A.*, 2012, **109**, 20443–20448.
8 E. W. Miller, J. Y. Lin, E. P. Frady, P. A. Steinbach, W. B. Kristan and R. Y. Tsien, *Proc. Natl. Acad. Sci. U. S. A.*, 2012, **109**, 2114–2119.
9 J. S. Treger, M. F. Priest, R. Iezzi and F. Bezanilla, *Biophys. J.*, 2014, **107**, L09–L12.
10 K. D. Piatkevich, E. E. Jung, C. Straub, C. Linghu, D. Park, H. J. Suk, D. R. Hochbaum, D. Goodwin, E. Pnevmatikakis, N. Pak, T. Kawashima, C. T. Yang, J. L. Rhoades, O. Shemesh, S. Asano, Y. G. Yoon, L. Freifeld, J. L. Saulnier, C. Riegler, F. Engert, T. Hughes, M. Drobizhev, B. Szabo, M. B. Ahrens, S. W. Flavell, B. L. Sabatini and E. S. Boyden, *Nat. Chem. Biol.*, 2018, **14**, 352–360.
11 D. R. Hochbaum, Y. Zhao, S. L. Farhi, N. Klapoetke, C. A. Werley, V. Kapoor, P. Zou, J. M. Kralj, D. Maclaurin, N. Smedemark-Margulies, J. L. Saulnier, G. L. Boulting, C. Straub, Y. K. Cho, M. Melkonian, G. K. Wong, D. J. Harrison, V. N. Murthy, B. L. Sabatini, E. S. Boyden, R. E. Campbell and A. E. Cohen, *Nat. Methods*, 2014, **11**, 825–833.
12 M. Kannan, G. Vasan, C. Huang, S. Haziza, J. Z. Li, H. Inan, M. J. Schnitzer and V. A. Pieribone, *Nat. Methods*, 2018, **15**, 1108–1116.
13 A. S. Abdelfattah, S. L. Farhi, Y. Zhao, D. Brinks, P. Zou, A. Ruangkittisakul, J. Platisa, V. A. Pieribone, K. Ballanyi, A. E. Cohen and R. E. Campbell, *J. Neurosci.*, 2016, **36**, 2458–2472.
14 L. Jin, Z. Han, J. Platisa, J. R. A. Wooltorton, L. B. Cohen and V. A. Pieribone, *Neuron*, 2012, **75**, 779–785.
15 Y. Gong, C. Huang, J. Z. Li, B. F. Grewe, Y. Zhang, S. Eismann and M. J. Schnitzer, *Science*, 2015, **350**, 1361–1366.
16 M. Z. Lin and M. J. Schnitzer, *Nat. Neurosci.*, 2016, **19**, 1142–1153.
17 J. Wu, Y. Liang, S. Chen, C.-L. Hsu, M. Chavarha, S. W. Evans, D. Shi, M. Z. Lin, K. K. Tsia and N. Ji, *Nat. Methods*, 2020, **17**, 287–290.
18 B. Chanda, R. Blunck, L. C. Faria, F. E. Schweizer, I. Mody and F. Bezanilla, *Nat. Neurosci.*, 2005, **8**, 1619–1626.
19 N. Ghitani, P. O. Bayguinov, Y. Ma and M. B. Jackson, *J. Neurophysiol.*, 2015, **113**, 1249–1259.
20 D. N. Ng and P. Fromherz, *ACS Chem. Biol.*, 2011, **6**, 444–451.
21 M. Sundukova, E. Prifti, A. Bucci, K. Kirillova, J. Serrao, L. Reymond, M. Umebayashi, R. Hovius, H. Riezman, K. Johnsson and P. A. Heppenstall, *Angew. Chem., Int. Ed.*, 2019, **58**, 2341–2344.
22 T. Fiala, J. Wang, M. Dunn, P. Šebej, S. J. Choi, E. C. Nwadibia, E. Fialova, D. M. Martinez, C. E. Cheetham, K. J. Fogle, M. J. Palladino, Z. Freyberg, D. Sulzer and D. Sames, *J. Am. Chem. Soc.*, 2020, **142**, 9285–9301.
23 A. S. Abdelfattah, T. Kawashima, A. Singh, O. Novak, H. Liu, Y. Shuai, Y.-C. Huang, L. Campagnola, S. C. Seeman, J. Yu, J. Zheng, J. B. Grimm, R. Patel, J. Friedrich, B. D. Mensh, L. Paninski, J. J. Macklin, G. J. Murphy, K. Podgorski, B.-J. Lin, T.-W. Chen, G. C. Turner, Z. Liu, M. Koyama, K. Svoboda, M. B. Ahrens, L. D. Lavis and E. R. Schreiter, *Science*, 2019, **365**, 699–704.
24 S. Liu, C. Lin, Y. Xu, H. Luo, L. Peng, X. Zeng, H. Zheng, P. R. Chen and P. Zou, *Nat. Chem.*, 2021, **13**, 472–479.
25 Y.-L. Huang, A. S. Walker and E. W. Miller, *J. Am. Chem. Soc.*, 2015, **137**, 10767–10776.
26 M. M. Milosevic, J. Jang, E. J. McKimm, M. H. Zhu and S. D. Antic, *eNeuro*, 2020, **7**, ENEURO.0060–0020.2020.
27 S. P. Ginebaugh, E. D. Cyphers, V. Lanka, G. Ortiz, E. W. Miller, R. Laghaei and S. D. Meriney, *J. Neurosci.*, 2020, **40**, 3504–3516.
28 A. Klimas, G. Ortiz, S. C. Boggess, E. W. Miller and E. Entcheva, *Prog. Biophys. Mol. Biol.*, 2020, **154**, 62–70.
29 H. M. McNamara, R. Salegame, Z. Al Tanoury, H. T. Xu, S. Begum, G. Ortiz, O. Pourquie and A. E. Cohen, *Nat. Phys.*, 2020, **16**, 357.
30 P. E. Deal, R. U. Kulkarni, S. H. Al-Abdullatif and E. W. Miller, *J. Am. Chem. Soc.*, 2016, **138**, 9085–9088.
31 P. E. Deal, P. Liu, S. H. Al-Abdullatif, V. R. Muller, K. Shamardani, H. Adesnik and E. W. Miller, *J. Am. Chem. Soc.*, 2020, **142**, 614–622.

32 S. R. Mujumdar, R. B. Mujumdar, C. M. Grant and A. S. Waggoner, *Bioconjugate Chem.*, 1996, **7**, 356–362.

33 Y. Koide, Y. Urano, K. Hanaoka, W. Piao, M. Kusakabe, N. Saito, T. Terai, T. Okabe and T. Nagano, *J. Am. Chem. Soc.*, 2012, **134**, 5029–5031.

34 B. Wang, X. Chai, W. Zhu, T. Wang and Q. Wu, *Chem. Commun.*, 2014, **50**, 14374–14377.

35 E. Kozma, G. Estrada Girona, G. Paci, E. A. Lemke and P. Kele, *Chem. Commun.*, 2017, **53**, 6696–6699.

36 C. R. Woodford, E. P. Frady, R. S. Smith, B. Morey, G. Canzi, S. F. Palida, R. C. Araneda, W. B. Kristan, C. P. Kubiak, E. W. Miller and R. Y. Tsien, *J. Am. Chem. Soc.*, 2015, **137**, 1817–1824.

37 T. K. Neklesa, H. S. Tae, A. R. Schneekloth, M. J. Stulberg, T. W. Corson, T. B. Sundberg, K. Raina, S. A. Holley and C. M. Crews, *Nat. Chem. Biol.*, 2011, **7**, 538–543.

38 H. Tabata and K. Nakajima, *Neuroscience*, 2001, **103**, 865–872.

39 Y. Koide, Y. Urano, K. Hanaoka, T. Terai and T. Nagano, *ACS Chem. Biol.*, 2011, **6**, 600–608.

40 J. B. Grimm, T. A. Brown, A. N. Tkachuk and L. D. Lavis, *ACS Cent. Sci.*, 2017, **3**, 975–985.

41 P. Liu, V. Grenier, W. Hong, V. R. Muller and E. W. Miller, *J. Am. Chem. Soc.*, 2017, **139**, 17334–17340.

42 G. Ortiz, P. Liu, S. H. H. Naing, V. R. Muller and E. W. Miller, *J. Am. Chem. Soc.*, 2019, **141**, 6631–6638.

43 V. Grenier, B. R. Daws, P. Liu and E. W. Miller, *J. Am. Chem. Soc.*, 2019, **141**, 1349–1358.

© 2021 The Author(s). Published by the Royal Society of Chemistry

RSC Chem. Biol., 2021, **2**, 1594–1599 | **1599**